Proc. of the European Safety and Reliability Conference (ESREL 2026)
Edited by José C. Matos, Paulo B. Lourenço, Michael Beer, Daniel Oliveira,
Edoardo Patelli, Hélder S. Sousa, Rui A. Silva and Monica Santamaria
 Published by Research Publishing, Singapore.
doi: 10.3850/ESREL2026061419_esrel26-p26394-cd

Severity-Graded, Step-Feature-Aware I–V Fault Diagnosis for PV Arrays: A Unified Rules + ML Pipeline

Bing Li[1 2], Xuejian Wang[2], Tong Zhao[2], Jian Hu[2], Yiqi Liu[1]
1 South China University of Technology, China. E-mail:aulyq@scut.edu.cn
2 Corporate Research Center, Midea, China. E-mail: {libing134, zhaotong10, jian1.hu}@midea.com

Photovoltaic arrays experience circuit faults (open/short), power-degradation faults (aging and potential-induced degradation), and current-mismatch faults (partial shading, hot spots, and cracking), each leaving a characteristic signature on current–voltage curves. We present a hybrid, multi-stage workflow that combines physics-informed features and rule-based logic with a lightweight learning back-end to deliver accurate, interpretable, and severity-graded diagnosis suitable for operations and maintenance. Preprocessing includes gap filling, outlier suppression, denoising, normalization by open-circuit voltage and short-circuit current, and irradiance/temperature compensation for fair comparison across modules. A step-aware segmentation module detects concave regions and step-like depressions associated with bypass-diode activation. We extract electrical descriptors (open-circuit voltage, short-circuit current, maximum-power-point voltage/current, and fill factor) and shape cues (end-region slope, step presence and depth, local goodness-of-fit around the step, and plateau slope). Diagnosis proceeds hierarchically: circuit-fault screening with severity grading, degradation identification via fill-factor reduction and end-region slope changes, and mismatch-subtype triage using plateau behavior and step-related current loss; when residual ambiguity remains (notably shading versus hot spots), a compact neural classifier provides a tie-break while preserving interpretability. Using the NIST photovoltaic monitoring dataset (six arrays; 2015–2018; minute-level sampling with current–voltage sweeps, irradiance, and temperature), we curate 167 illustrative traces for validation and demonstrate robust multi-fault coverage, fine-grained mismatch triage, and clear severity grading.

Keywords: Photovoltaics; I–V curve; step features; fault diagnosis; severity grading

1. Introduction

Large-scale PV plants face persistent O&M challenges: manual inspection is labour-intensive, costly, and struggles with hidden or dispersed fault sources; data silos across SCADA, weather, and device signals further hamper holistic analytics. A data-driven yet interpretable I–V-based diagnosis can raise efficiency and shorten fault remediation cycles. This paper presents an engineering-ready workflow that (i) covers multiple fault families in one pipeline, (ii) produces severity-graded outputs for maintenance prioritization, and (iii) remains interpretable for field engineers. We combine rules grounded in physical meanings with lightweight learning modules to improve difficult distinctions such as partial shading vs. hot spots. The proposed approach is tailored for EMS integration and remote I–V scanning environments.

Contributions

- A unified three-stage diagnostic flow (circuit → aging/PID → mismatch subtype) that couples rules with learning.
- A step-feature-aware segmentation that uses step presence/depth, Slope2, and local R^2 to separate shading, hot spot, and cracking.
- Severity grading tied to physically meaningful deviations (Isc/Voc, FF, step current drop), producing O&M-actionable reports.

2. Related Work

Signal conditioning often uses local polynomial smoothing (Savitzky–Golay) to reduce noise without distorting curvature (Savitzky and Golay 1964). The single-diode equivalent model remains a standard for PV I–V behaviour and parameter estimation (Villalva, Gazoli, and Ruppert Filho 2009). PID mechanisms and impacts have been comprehensively reviewed (Luo et al. 2017), highlighting performance loss and reliability concerns. Under partial shading, bypass-diode activation produces step-like

depressions and may lead to hot-spot stress (Vieira et al. 2020); extensive studies discuss mitigation and reliability.

3. Background and Problem Statement

We consider three fault families: (a) circuit faults (open/short), (b) power-degradation faults (aging, PID), and (c) current-mismatch faults (partial shading, hot spots, cracking/glass damage). These families manifest distinct I–V patterns that can be characterized by a concise set of electrical and morphological features. The task is: given a measured I–V curve with context (irradiance, temperature), infer the fault type and its severity (mild/moderate/severe) with interpretable evidence in the form of salient features and thresholds.

4. Methodology

4.1. System Architecture and Modules

The proposed workflow comprises six modules arranged in a unidirectional pipeline: data ingestion and environmental compensation; signal preprocessing; step-aware curve segmentation; feature engineering; rule-based diagnosis with severity grading; and an optional learning refiner. Raw I–V sweeps are standardized (sampling order, physical validity, environmental comparability), denoised, and normalized to enable cross-module comparability. Segmentation then identifies step-like depressions associated with bypass-diode activation. A compact set of electrical and morphological features is computed and fed to a three-stage rule system that (i) detects circuit faults, (ii) separates aging and PID, and (iii) disambiguates current-mismatch subtypes. When rule evidence is inconclusive (e.g., partial shading vs. hot spot), an optional lightweight learner provides a tie-break while preserving the overall explainability of the decision path.

4.2. Preprocessing

Given a raw sweep $\{(V_k, I_k)\}_{k=1}^{N}$, we first enforce physical and sampling consistency. Samples with $V_k<0$ or $I_k<0$ are discarded, and the sequence is strictly ordered by voltage to preserve a single-valued $I(V)$ relation. Missing points arising from sensor dropouts are imputed by linear interpolation on V, using nearest-neighbour extrapolation at the boundaries to maintain cardinality.

To suppress measurement noise while preserving curvature, we employ short-support filters. A Savitzky–Golay filter (typical parameters window length 3, polynomial order 3) is used to reduce high-frequency noise with minimal phase distortion; for impulsive disturbances we substitute a median filter of comparable span, and for mild stationary noise a mean filter of the same support. Filter choice is thus matched to the dominant noise characteristic inferred from simple diagnostics (e.g., local variance and outlier rate).

Because open-circuit voltage V_{oc} and short-circuit current I_{sc} vary across modules and conditions, voltage and current are normalized by their contemporaneous (V_{oc}, I_{sc}) estimates to $\tilde{V} \in [0,1]$ and $\tilde{I} \in [0,1]$. For consistent sampling density, the curve is then resampled on an equal-$\Delta\tilde{V}$ grid with linear interpolation of $\tilde{I}$. When low-voltage segments contain gaps or excessive noise, we optionally fit a single-diode model to the sweep and use the fit to regularize or backfill missing values; the estimated series and shunt resistances (R_s, R_p) are retained as auxiliary physics-based descriptors for degradation analysis. Finally, irradiance and temperature compensation is applied to approximate STC-equivalent behavior, which stabilizes thresholds used later for rule decisions.

4.3. Step-Aware Curve Segmentation

Step-like current depressions are indicative of bypass-diode activation and are central to mismatch triage. We detect these regions using a local concavity test. For a sliding window $W = \{(V_a,I_a), (V_m,I_m), (V_b,I_b)\}$ with mid-point m, we compute the chord joining (V_a,I_a) and (V_b,I_b) and define the deviation in Eq.(1):

$$\Delta I_m = I_m - I_{line}(V_m). \quad (1)$$

Concave depressions produce $\Delta I_m<0$. To improve separability under small $|\Delta I_m|$, we apply an amplitude-selective magnifier in Eq.(2):

$$M(\Delta I_m) = -\Delta I_m \exp(10\,\Delta I_m), \quad (2)$$

which preserves sign while accentuating meaningful drops. Consecutive windows with consistent concavity are merged into candidate

segments. Each candidate is then validated by a local linear-fit test: points within the segment (and a small margin) are regressed against a line; segments with goodness-of-fit R^2 below a threshold are retained as significant depressions. For confirmed steps, we record (i) the pre-step "first linear" slope near open circuit (Slope1), (ii) the plateau slope across the step (Slope2), (iii) the step depth (current loss relative to the local chord), and (iv) the local R^2 around the concavity, which is empirically sensitive to cracking/glass damage.

4.4 Feature Engineering

From each standardized trace we compute electrical features—V_{oc}, I_{sc}, V_{mpp}, I_{mpp}, and fill factor $FF=(V_{mpp}I_{mpp})/(V_{oc}I_{sc})$ and morphological descriptors derived from the segmentation: Slope1 near the open-circuit end, binary step presence and step depth, local R^2 in the concave zone, and Slope2 on the post-step plateau. Environmental compensation ensures that all features are comparable across modules and seasons, enabling global thresholds with optional site-level adaptation.

4.5 Rule-Based Diagnosis with Severity Grading

Diagnosis proceeds hierarchically. Stage-1 screens for circuit faults using compensated V_{oc} and I_{sc}, depressed V_{oc} suggests open-circuit behavior, whereas suppressed I_{sc} indicates short-circuit conditions. Severity is mapped from the absolute deviation relative to nominal references. Stage-2 separates aging and PID: aging primarily manifests as a reduction in FF (and depressed V_{mpp}, I_{mpp}), while PID increases Slope1 near the open-circuit end; severity is graded by the magnitudes of FF drop and Slope1 elevation. Stage-3 activates only when a step is present. Shallow plateaus with gentle Slope2 are typical of partial shading; steeper Slope2 with confined loss suggests hot spots; low local R^2 alongside step loss is consistent with cracking or glass damage. Severity is proportional to step-related current loss.

4.6 Optional Learning Refiner

A small BP network with an SVM tie-breaker is invoked only when Stage-3 ambiguity remains (commonly shading vs. hot spot). This design preserves a rule-first, explainable backbone while improving edge cases with minimal computational overhead.

4.7 Threshold Calibration and Site Adaptation

Although global thresholds perform well under compensation, site-specific adaptation improves robustness. We estimate nominal references by robust statistics (e.g., median and inter-quartile ranges) and detect outliers by quantile or 3σ rules. When operating regimes are multi-modal (e.g., seasonal irradiance clusters), unsupervised clustering is used to partition regimes before deriving local thresholds. The severity mapping functions (e.g., for FF drop, Slope1 delta, step loss) are then calibrated per site.

5. *Experiment Design*

Goals. Evaluate (G1) **feature separability** for each fault family, (G2) **consistency** of severity grading, (G3) **robustness** of step detection under noise and environmental variation, and (G4) **runtime suitability** for EMS-side deployment.

Dataset & subset. We use **NIST PV** data (2015–2018; minute-level telemetry and I–V sweeps). We curated **167 I–V sweeps** from *canopy_East* (1st/15th each month; morning/noon/afternoon) to span diverse conditions (Boyd et al. 2017; NIST 2026).

Procedures.

1) **Preconditioning:** filtering, interpolation, denoising (SG/median/mean), V_{oc}/I_{sc} normalization, equal-ΔV resampling, irradiance/temperature compensation.
2) **Segmentation & features:** step detection with concavity + local R^2; features $\{V_{oc}, I_{sc}, V_{mpp}, I_{mpp}, FF$, Slope1, Slope2, step depth, $R^2\}$.
3) **Rules:** 3-stage thresholds; FF/V_{mpp} gate for normal vs. aging; Slope1 for PID; Slope2/R^2/step depth for mismatch subtypes; severity from deviation/loss.
4) **Statistics**: For (G1), two-sample *t*-tests (Welch) on selected pairs (e.g., normal vs. aging on FF/V_{mpp}), reporting *p-values*; for (G2), monotonicity checks between severity labels and feature magnitudes; for (G3), visual confirmation on exemplars; for (G4), big-O module complexity and measured CPU runtimes (single sweep).

Baselines. (B1) **Threshold-only** without environmental compensation; (B2) **No step segmentation** (global features only).

6. *Results*

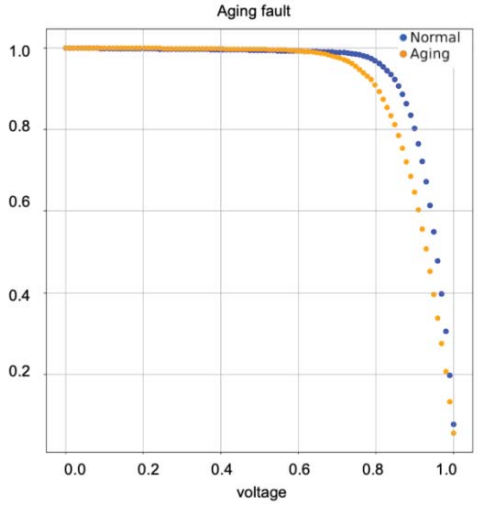

Figure 1 — Aging exemplars (normal → mild/moderate/severe).

This figure contrasts a normal module against aging cases at increasing severity. Aging manifests as a downward displacement of the I–V trace around the MPP, with a corresponding drop in fill factor (FF) and typically reduced V_{mpp} and I_{mpp}. In our workflow, FF loss is the primary severity indicator: small ΔFF is labelled mild, while larger ΔFF maps to moderate and severe. The visual MPP depression in the exemplars aligns with the monotonic FF decrease used by the rule set.

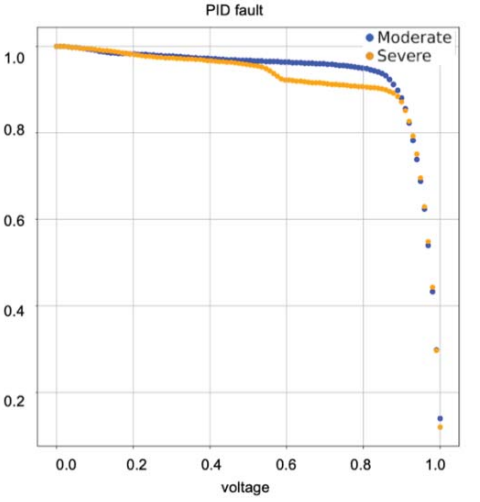

Figure 2 — PID exemplars (moderate vs. severe).

As shown in figure 2, potential-induced degradation is illustrated with two traces of different severity. Relative to a normal curve, the end-slope near the low-voltage (short-circuit) side increases under PID, producing a sharper rise of current as $V \to 0$. We quantify this with the near-end slope increment (defined in Methods) and assign severity by the magnitude of this increment: the moderate case shows a clear but smaller increase, whereas the severe case exhibits a pronounced steepening. This end-slope change is the principal cue used by our rules to flag PID and grade its impact.

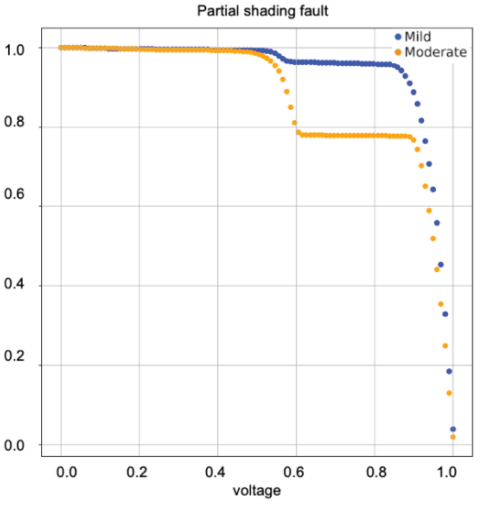

Figure 3 — Partial shading exemplars (mismatch: step present, gentle plateau).

Figure 3 shows that partial shading produces a step-like depression in the I–V curve due to bypass-diode activation. The exemplars show a gentle post-step plateau slope (shallow Slope2), characteristic of shading rather than hotspot heating. Within this family, we use the step current loss ("step depth") as a monotonic severity measure: smaller losses correspond to *mild* shading, while larger losses indicate *moderate* to *severe* cases. The shape and depth of the step in the figure are consistent with the rule-based subtype and severity assignments.

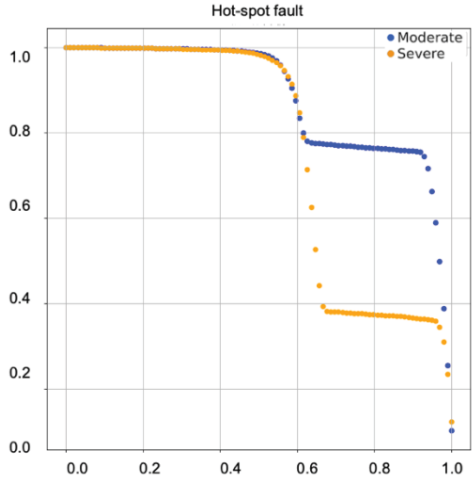

Figure 4 — Hot-spot exemplars (mismatch: step present, steeper plateau).

In figure 4 hot spots also exhibit the step signature, but the plateau beyond the step is steeper (larger Slope2) than in partial shading, reflecting stronger localized stress. As in shading, step depth drives the severity grade; however, the steeper plateau in these exemplars is the discriminative cue that separates hot spots from partial shading in our Stage-3 logic. The displayed *moderate* and *severe* cases show progressively larger step losses and steeper post-step slopes, in line with the rule thresholds used by the classifier.

Together, Figures 1–4 span the full severity ladder (normal, mild, moderate, severe) across aging, PID, and mismatch subtypes. The visual signatures—MPP depression (aging), end-slope increase (PID), and step formation plus plateau slope (mismatch)—match the features used by our decision rules, yielding consistent, interpretable grading.

Scalability: the end-to-end pipeline is linear in the number of sampled points per sweep because preprocessing, step-aware segmentation (sliding-window concavity tests plus local linear fits), and feature extraction each make a single pass over the curve. The rule-based stages add constant overhead, and the optional learning refiner is invoked only for a small subset of ambiguous mismatch cases. As a result, the approach scales to high-frequency remote scanning and multi-string monitoring by parallelizing over sweeps (or strings) and by streaming computation per sweep without retaining long histories.

Transferability: the method is largely technology-agnostic because it relies on normalized electrical descriptors and curve-shape evidence rather than device-specific parameters. It transfers naturally across different module ratings and array sizes via normalization and environmental compensation, while site adaptation can be achieved by re-estimating nominal references and thresholds using robust statistics on a short period of healthy-operation data. For technologies with different curve knees or bypass-diode configurations (e.g., thin-film or special string layouts), the same feature set can be retained but the decision thresholds and the mismatch tie-break model should be recalibrated using a small local calibration set. This provides a practical path to extending the workflow to other photovoltaic technologies and deployment sites without re-designing the full pipeline.

7. Engineering Integration

The workflow's **explainable rules** and **compact features** allow deployment as an EMS-side microservice that ingests I–V sweeps plus weather, runs **Stage-1→2→3** with **severity**, and emits **actionable reports** (fault type, severity, feature evidence, and suggested follow-ups). The system aligns with remote I–V scans and can fuse SCADA/weather feeds.

8. Limitations and Future Work

NIST data lack **ground-truth fault labels**; our study emphasizes feature separability, rule calibration, and qualitative validation on curated

traces. We plan (i) larger labelled corpora from field campaigns, (ii) robust STC normalization and explicit R_s/R_p tracking for degradation, and (iii) extended mismatch logic for multiple substring activations.

9. Conclusion

We introduced a **severity-graded, step-aware** I–V diagnosis that unifies circuit, degradation, and mismatch faults in a rule-first pipeline with optional learning. On curated NIST traces, the method shows clear separability, robust step detection, and actionable severity mapping, fitting real-world O&M and EMS integration.

References

Savitzky, Abraham, and Marcel J. E. Golay. 1964. "Smoothing and Differentiation of Data by Simplified Least Squares Procedures." *Analytical Chemistry* 36 (8): 1627–39.

Villalva, M.G., J.R. Gazoli, and E. Ruppert Filho. "Comprehensive Approach to Modeling and Simulation of Photovoltaic Arrays." *IEEE Transactions on Power Electronics* 24, no. 5 (2009): 1198–1208.

Luo, W., et al. "Potential-Induced Degradation in Photovoltaic Modules." *Energy & Environmental Science* 10 (2017): 43–68.

Vieira, R.G., et al. "A Comprehensive Review on Bypass Diode Application on Photovoltaic Modules." *Energies* 13, no. 10 (2020): 2472.

NIST. *Photovoltaic Data.* Accessed Jan 2026. https://pvdata.nist.gov/

Boyd, M., et al. "Performance Data from the NIST Photovoltaic Arrays and Associated Weather Station." *Journal of Research of NIST* 122 (2017).